Comparing the Mechanism and Energetics of CO_2 Sorption in the SIFSIX Series

Katherine A. Forrest,[†,§] Tony Pham,[*,†,§] Brian Space[*,†]
[†]*Department of Chemistry, University of South Florida,*
4202 East Fowler Avenue, CHE205, Tampa, FL 33620-5250, United States
[§]Authors contributed equally
[*]brian.b.space@gmail.com; tpham4@mail.usf.edu

SIFSIX Series

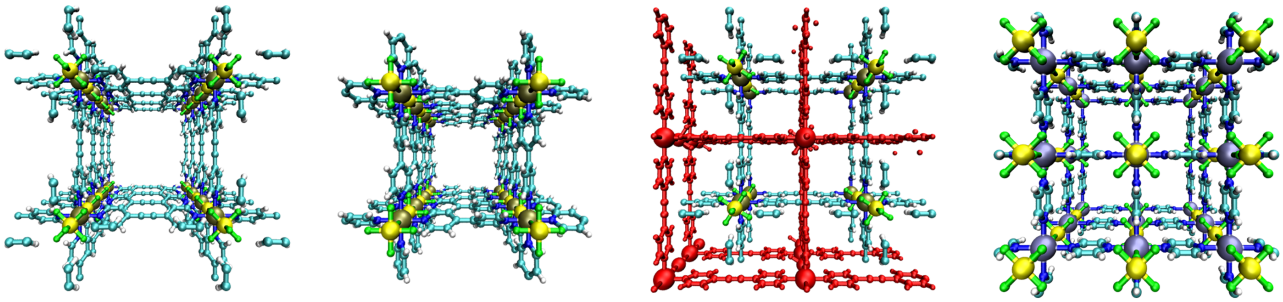

	SIFSIX-2-Cu	**SIFSIX-1-Cu**	**SIFSIX-2-Cu-i**	**SIFSIX-3-Zn/Cu**
Pore Size (Å):	13.05	9.54	5.15	3.84/3.54

Figure S1. Representations of the crystal structures for the different members of the SIFSIX series: **SIFSIX-2-Cu**, **SIFSIX-1-Cu**, **SIFSIX-2-Cu-i**, **SIFSIX-3-Zn**, and **SIFSIX-3-Cu**. Note, in **SIFSIX-2-Cu-i**, the red net represents the interpenetrated net. The pore size, defined as the longest channel diagonal distance minus the distance corresponding to van der Waals radii, for each MOM is also listed. Atom colors: C = cyan, H = white, N = blue, F = green, Si = yellow, Cu = tan, Zn = lavender.

Grand Canonical Monte Carlo

Simulations of CO_2 sorption in all five SIFSIX MOMs were performed using grand canonical Monte Carlo (GCMC) methods[1] within the crystal structure of the respective MOMs. The chemical potential potential (μ), volume (V), and temperature (T) were held constant within these simulations, while the particle number (N) was allowed to vary. For **SIFSIX-1-Cu**, **SIFSIX-2-Cu**, **SIFSIX-2-Cu-i**, **SIFSIX-3-Zn** and **SIFSIX-3-Cu**, the parametrizations and simulations were performed within the crystal structure published in reference 2, 3, 3, 4, and 5, respectively. System cell dimensions of $2 \times 2 \times 4$ were used for the simulations in **SIFSIX-1-Cu**, **SIFSIX-2-Cu**, and **SIFSIX-2-Cu-i**, while $3 \times 3 \times 3$ system cells were used for **SIFSIX-3-Zn** and **SIFSIX-3-Cu**. For each MOM, a spherical cut-off distance (R_c) corresponding to half the shortest system cell dimension length was used for the simulations (**SIFSIX-1-Cu** = 11.045 Å, **SIFSIX-2-Cu** = 13.6316 Å, **SIFSIX-2-Cu-i** = 13.649 Å, **SIFSIX-3-Zn** = 10.711 Å, **SIFSIX-3-Cu** = 10.3779 Å). Note, we also simulated CO_2 sorption in **SIFSIX-2-Cu-i** using a $2 \times 2 \times 2$ system cell of the MOM (R_c = 8.092 Å) and these results are compared with those for the larger system cell in Figure S10. All MOM atoms were kept fixed throughout the simulations. In GCMC, the average particle number ($\langle N \rangle$) was calculated by the following statistical mechanical equation:[6,7]

$$\langle N \rangle = \frac{1}{\Xi} \sum_{N=0}^{\infty} e^{\beta \mu N} \left\{ \prod_{i=1}^{3N} \int_{-\infty}^{\infty} dx_i \right\} N e^{-\beta U(x_1, \ldots x_{3N})} \tag{1}$$

where Ξ is the grand canonical partition function, β is the quantity $1/kT$ (k is the Boltzmann constant), and U is the total potential energy. μ for CO_2 was determined for a range of temperatures and pressures through the Peng-Robinson equation of state.[8] In this work, the total potential energy of the MOM–CO_2 system was calculated through the sum of the repulsion/dispersion energy as calculated using the Lennard-Jones 12–6 potential,[9] the electrostatic energy as calculated *via* Ewald summation,[10,11] and the many-body polarization energy as calculated using a Thole–Applequist type model.[12–15] The repulsion/dispersion interactions between unlike species were governed by the Lorentz–Bertholet mixing rules.[16] Details for obtaining the repulsion/dispersion, electrostatic, and polarizability parameters for the MOM atoms are described in the subsequent sections. CO_2 was modeled as a rigid five–site polarizable potential that was developed previously.[17] Long-range corrections were applied to all terms of the potential energy to reduce finite-size effects; this included using a previously reported procedure for the repulsion/dispersion energy[18] and direct Wolf summation for the polarization energy.[19] Once $\langle N \rangle$ was calculated, it was converted to a value that can be compared with experimentally. In GCMC, the Q_{st} values were calculated using the following statistical mechanical expression that involves fluctuations in N and U:[20]

$$Q_{st} = -\frac{\langle NU \rangle - \langle N \rangle \langle U \rangle}{\langle N^2 \rangle - \langle N \rangle^2} + kT \tag{2}$$

The Massively Parallel Monte Carlo (MPMC) code,[21] an open-source code that is currently available for download on GitHub, was used to perform the simulations in this work. For all state points considered in each MOM, the simulations consisted of at least 5×10^6 Monte Carlo steps to guarantee equilibration, followed by an additional 5×10^6 steps to sample the desired thermodynamic properties.

Repulsion/Dispersion and Polarizabilities

For all five SIFSIX MOM atoms investigated in this work, the repulsion/dispersion parameters (Lennard–Jones ϵ and σ) for all C, H, and N atoms were taken from the Optimized Potentials for Liquid Simulations – All Atom (OPLS-AA) force field.[22] This force field includes parameters that are specific for aromatic systems, which all of these MOMs contains. As for the F, Si, Cu (in **SIFSIX-1-Cu**, **SIFSIX-2-Cu**, **SIFSIX-2-Cu-i**, and **SIFSIX-3-Cu**) and Zn (in **SIFSIX-3-Zn**) atoms, the repulsion/dispersion parameters from the Universal Force Field (UFF) were assigned to these atoms as the OPLS force field do not contain parameters for such atoms.

The atomic point polarizabilities for all C, H, N, and F atoms were taken from a highly transferable set provided by the work of van Duijnen and Swart.[23] The polarizability parameter for Si^{4+}, Cu^{2+}, and Zn^{2+} were not included in the aforementioned set, so the parameters for these ions were determined by fitting a molecular polarizability tensor to one that was obtained from quantum mechanical calculations for fragments containing the respective ions. The parameters for these ions were determined in previous work by our group (Si^{4+} = 2.13300 Å^3, Cu^{2+} = 2.19630 Å^3, Zn^{2+} = 1.98870 Å^3)[24–28] and they were used for the simulations performed herein. Polarizabilities were assigned to the nuclear center of all atoms of the respective MOMs to model explicit many-body polarization, which was executed using a Thole–Applequist type model.[12–15]

Partial Charges For SIFSIX-1-Cu

In this work, the calculations and simulations in **SIFSIX-1-Cu** were performed in the 4,4′-bipyridine (bpy) ring configuration in which orthogonal pyridyl rings are facing one another within a unit cell as shown in Figure S2(a). Further, the position of the equatorial fluorine atoms was chosen such that these atoms are eclisped with the pyridyl N atoms as shown in Figure S2(b) This selection of the bpy ring configuration and the equatorial fluorine atom position for **SIFSIX-1-Cu** yielded the highest CO_2 uptake for simulations in this MOM.[27] The orientation of the pyridyl rings in the configuration chosen allows the sorbate molecules to have the best access to the $SiF_6{}^{2-}$ pillars. In addition, by having the equatorial fluorine atoms eclipsed with the square grid, a single CO_2 molecule can interact with two equatorial fluorine atoms of the $SiF_6{}^{2-}$ group simultaneously (Figure S11), which is a highly favorable interaction that corresponds to the initial isosteric heat of adsorption (Q_{st}) for CO_2 in this MOM.

The partial charges for the 10 chemically distinct atoms in **SIFSIX-1-Cu** (Figure S3) were determined through electronic structure calculations on a variety of fragments that were extracted from the crystal structure of the MOM. The fragments that were considered in this work for **SIFSIX-1-Cu** are displayed in Figure S4. The NWChem *ab initio* simulation software[29] was used to calculate the electrostatic potential surface (ESP) at the Hartree–Fock level of theory for each fragment. For these calculations, all C, H, N, F, and Si atoms were treated with the 6-31G* basis set to produce overpolarized charges that are appropriate for condensed phase simulation,[30] while the LANL2DZ ECP basis set[31–33] was assigned to the Cu^{2+} ions for proper treatment of the inner electrons of this species. The partial charges were fitted onto the atomic centers to reproduce the ESP of the fragment; this was executed using the CHELPG method.[34,35]

The calculated average partial charges for each chemically distinct atom within the selected fragments for **SIFSIX-1-Cu** are provided in Table S1. Note, atoms that are buried or located on the edges were not included in the averaging. The partial charges for all chemically distinct atoms were averaged between the fragments. The charges were then adjusted so that the total charge of the framework was neutral. The resulting partial charges for each chemically distinct atom in **SIFSIX-1-Cu** are shown in Table S2. We note that the partial charges for the chemically distinct atoms in MOMs can also be determined through periodic fitting of the entire crystal structure.[36,37] However, due to the presence of buried atoms in the crystal structure of the SIFSIX MOMs, these calculations resulted in underdetermined atomic partial charges for some of these materials. Nevertheless, this method was successfully used to calculate sensible partial charges for the unique atoms in **SIFSIX-1-Cu** in previous work and such charges are reported therein.[27]

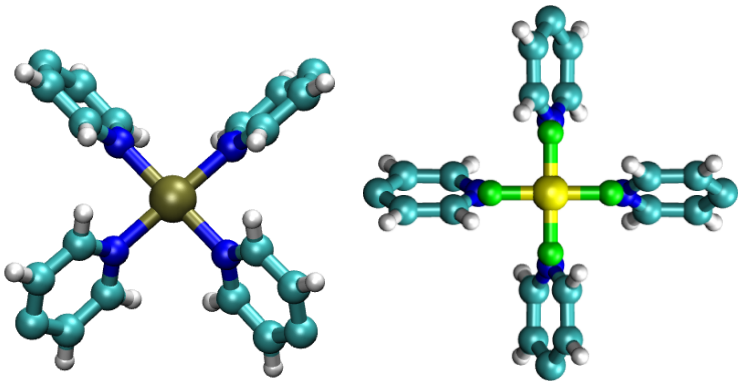

(a) (b)

Figure S2. (a) A top view unit cell representation showing **(a)** the 4,4′-bipyridine (bpy) ring configuration and **(b)** the equatorial fluorine atom position of **SIFSIX-1-Cu** used for the simulations in this work. In **(a)**, the bpy ring configuration consists of pyridyl rings that are twisted with respect to each other and where two orthogonal pyridyl rings are facing one another. In **(b)**, the equatorial fluorine atoms are eclipsed with the pyridyl nitrogen atoms. Atom colors: C = cyan, H = white, N = blue, F = green, Si = yellow, Cu = tan.

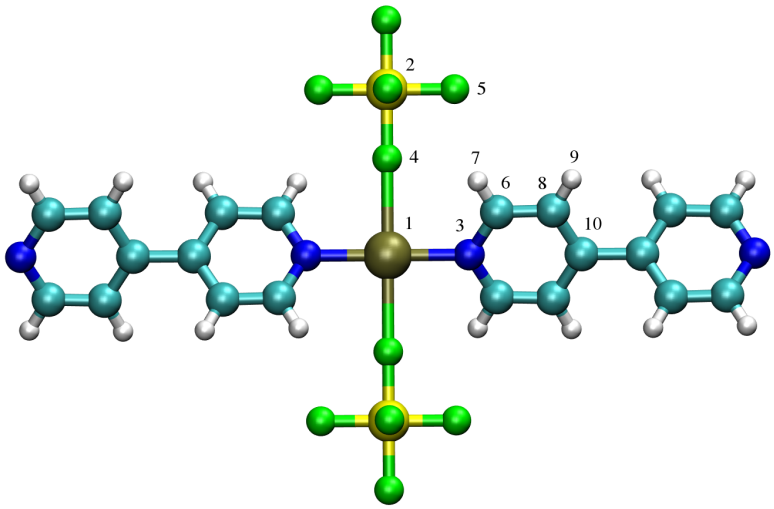

Figure S3. The numbering of the chemically distinct atoms in **SIFSIX-1-Cu** as referred to in Tables S1 and S2. Atom colors: C = cyan, H = white, N = blue, F = green, Si = yellow, Cu = tan.

Table S1. Comparison of partial charges (e^-) for the series of fragments that were selected for **SIFSIX-1-Cu** as listed in Figure S4. Label of atoms corresponds to Figure S3.

Atom	Label	Frag 1	Frag 2	Frag 3	Frag 4	Frag 5	Frag 6
Cu	1	-	-	0.5089	1.1741	-	0.2555
Si	2	1.5364	1.6023	1.7626	1.7653	1.6512	1.7667
N	3	-0.2086	-0.3647	-0.2126	-	-	-0.4028
F	4	-0.5845	-0.5838	-0.6160	-0.5932	-0.6037	-0.6199
F	5	-0.5775	-0.5700	-0.6050	-0.6015	-0.5959	-0.6052
C	6	0.1098	0.0692	0.1967	0.2795	0.1409	0.1917
H	7	0.1801	0.1673	0.1582	0.1323	0.1779	0.1619
C	8	-0.3732	-0.3114	-0.3586	-0.3667	-0.3865	-0.3487
H	9	0.2013	0.1890	0.1987	0.2001	0.1871	0.1818
C	10	0.1607	0.2306	0.2077	0.2390	0.2748	0.2383

Table S2. The partial charges (e^-) for the chemically distinct atoms in **SIFSIX-1-Cu**. Label of atoms correspond to Figure S3.

Atom	Label	q (e^-)
Cu	1	0.64630
Si	2	1.68070
N	3	-0.28830
F	4	-0.58230
F	5	-0.57490
C	6	0.16460
H	7	0.16290
C	8	-0.34680
H	9	0.19300
C	10	0.22520

Figure S4. Fragments of **SIFSIX-1-Cu** that were selected for gas phase charge fitting calculations. Label of atoms correspond to Figure S3. Atom colors: C = cyan, H = white, N = blue, F = green, Si = yellow, Cu = tan.

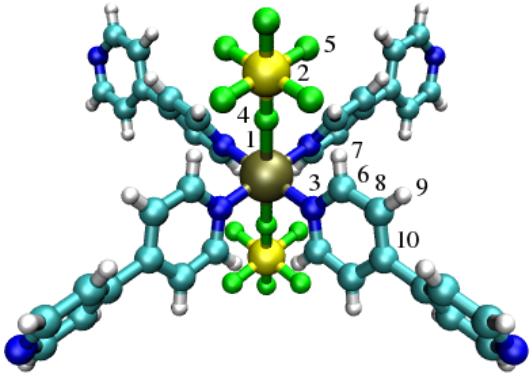

(a) Fragment 1

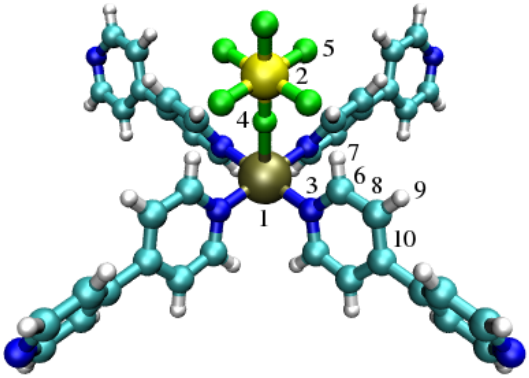

(b) Fragment 2

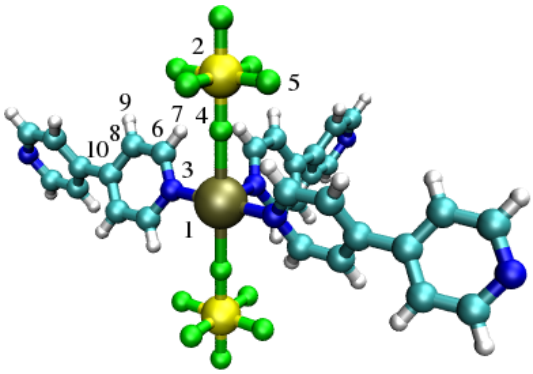

(c) Fragment 3

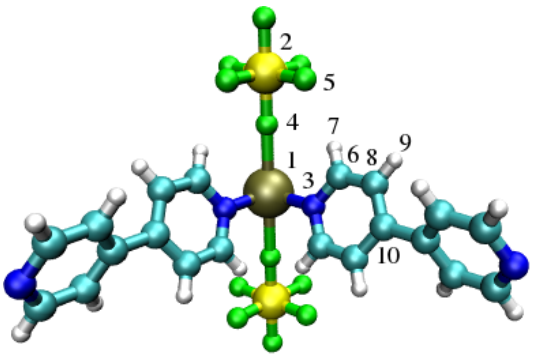

(d) Fragment 4

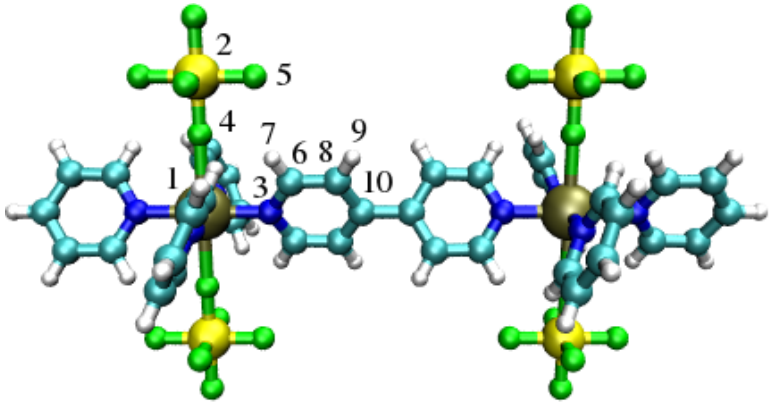

(e) Fragment 5

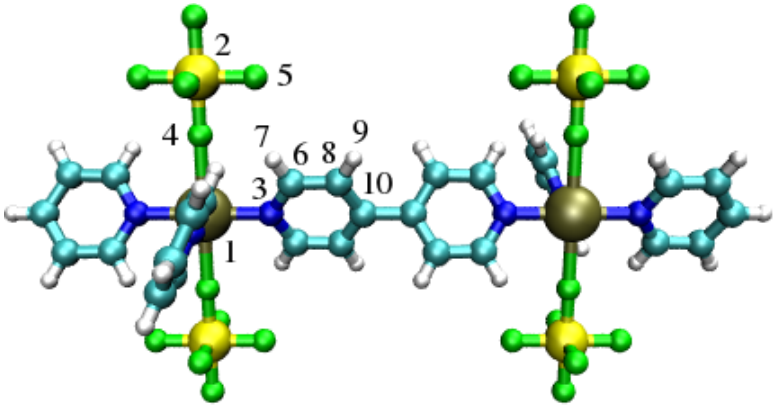

(f) Fragment 6

Partial Charges For SIFSIX-2-Cu and SIFSIX-2-Cu-i

The partial charges for the 11 chemically distinct atoms in **SIFSIX-2-Cu** and **SIFSIX-2-Cu-i** (Figure S5) were determined using the same methods as described in the previous section. The fragments that were selected for **SIFSIX-2-Cu-i** can be found in previous work.[25] Fragments of similar type to those chosen for **SIFSIX-2-Cu-i** were also used for the electronic structure calculations for **SIFSIX-2-Cu**. The partial charges for each chemically distinct atom for both **SIFSIX-2-Cu** and **SIFSIX-2-Cu-i** can be found in Table S3. It can be observed that the partial charges for each unique atom are very similar between the two polymorphs.

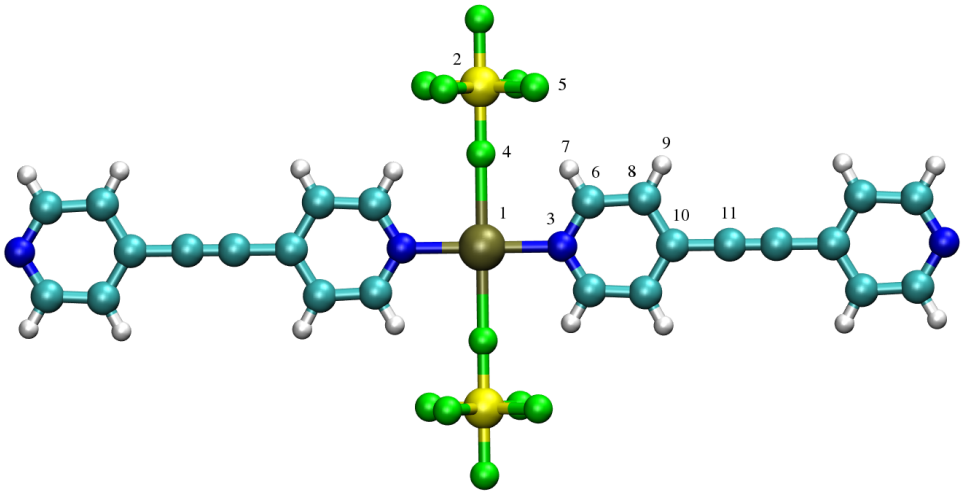

Figure S5. The numbering of the chemically distinct atoms in **SIFSIX-2-Cu** and **SIFSIX-2-Cu-i** as referred to in Table S3. Atom colors: C = cyan, H = white, N = blue, F = green, Si = yellow, Cu = tan.

Table S3. The partial charges (e^-) for the chemically distinct atoms in **SIFSIX-2-Cu** and **SIFSIX-2-Cu-i**. Label of atoms correspond to Figure S5.

Atom	Label	**SIFSIX-2-Cu** q (e^-)	**SIFSIX-2-Cu-i** q (e^-)
Cu	1	0.32090	0.28930
Si	2	1.60950	1.58870
N	3	-0.08740	-0.05720
F	4	-0.51920	-0.53420
F	5	-0.56250	-0.56270
C	6	0.16080	0.14510
H	7	0.16770	0.15800
C	8	-0.30530	-0.32090
H	9	0.17900	0.17810
C	10	0.21470	0.25390
C	11	-0.19220	-0.15700

Partial Charges For SIFSIX-3-Zn

The partial charges for the 7 chemically distinct atoms in **SIFSIX-3-Zn** (Figure S6) were determined using the same methods as implemented in the previous two sections. The fragments that were selected for **SIFSIX-3-Zn** can be found in previous work.[26] As with the Cu^{2+} ions, the LANL2DZ ECP basis set[31–33] was used to treat the Zn^{2+} ions for the electronic structure calculations. The partial charges for all chemically distinguishable atoms in **SIFSIX-3-Zn** can be found in Table S4.

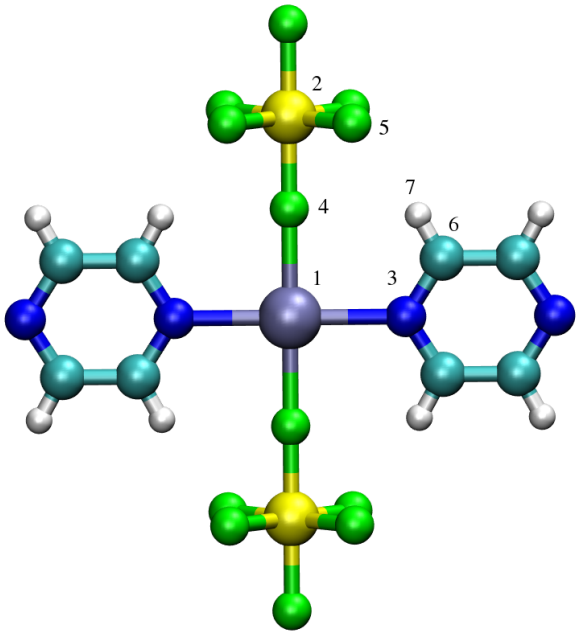

Figure S6. The numbering of the chemically distinct atoms in **SIFSIX-3-Zn** as referred to in Table S4. Atom colors: C = cyan, H = white, N = blue, F = green, Si = yellow, Zn = lavender.

Table S4. The partial charges (e^-) for the chemically distinct atoms in **SIFSIX-3-Zn**. Label of atoms correspond to Figure S6.

Atom	Label	q (e^-)
Zn	1	0.97253
Si	2	1.75079
N	3	-0.30470
F	4	-0.55344
F	5	-0.56285
C	6	0.11496
H	7	0.11676

Partial Charges For SIFSIX-3-Cu

The partial charges for the 7 chemically distinct atoms in **SIFSIX-3-Cu** (Figure S7) were determined using the same methods as described above for **SIFSIX-1-Cu**, **SIFSIX-2-Cu**, and **SIFSIX-2-Cu-i**. The fragments that were selected for **SIFSIX-3-Cu** are shown in Figure S8; these are very similar to those that were chosen for **SIFSIX-3-Zn**.[26] The partial charges for each chemically distinct atom within the fragments are provided in Table S5. The final tabulated partial charges for each unique atom in **SIFSIX-3-Cu** are listed in Figure S6. When comparing the partial charges between **SIFSIX-3-Zn** and **SIFSIX-3-Cu**, it can be observed from an electrostatics point of view that substitution of Zn^{2+} with Cu^{2+} causes the equatorial fluorine atoms (atom labeled 5 in Figures S6 and S7) to be slightly more negatively charged.

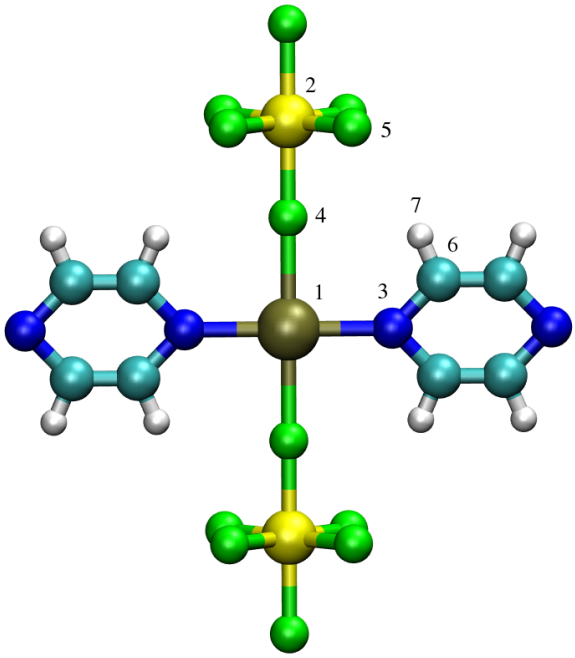

Figure S7. The numbering of the chemically distinct atoms in **SIFSIX-3-Cu** as referred to in Tables S5 and S6. Atom colors: C = cyan, H = white, N = blue, F = green, Si = yellow, Cu = tan.

Table S5. Comparison of partial charges (e^-) for the series of fragments that were selected for **SIFSIX-3-Cu** as listed in Figure S8. Label of atoms corresponds to Figure S7.

Atom	Label	Frag 1	Frag 2	Frag 3	Frag 4	Frag 5	Frag 6	Frag 7	Frag 8	Frag 9	Frag 10
Cu	1	-	0.2093	0.3463	-	-	0.3118	0.5868	-	0.1317	0.9648
Si	2	1.8695	1.9353	1.8214	1.8235	1.8225	1.8312	1.7715	1.7748	1.8565	1.8451
N	3	0.0830	-0.0835	-0.0939	-0.1082	0.1456	-0.0795	-0.3495	0.1345	-0.0709	-0.2143
F	4	-0.6625	-0.6430	-0.6565	-0.6114	-0.6585	-0.6020	-0.6278	-0.6604	-0.6645	-0.6194
F	5	-0.6136	-0.6076	-0.5936	-0.5933	-0.6021	-0.5913	-0.5787	-0.6075	-0.5983	-0.5871
C	6	0.0292	0.0658	0.0696	0.1379	0.0188	0.0780	-	-0.0428	0.0731	0.1243
H	7	0.1857	0.1463	0.1557	0.1358	0.1822	0.1349	-	0.1938	0.1457	0.1156

Table S6. The partial charges (e^-) for the chemically distinct atoms in **SIFSIX-3-Cu**. Label of atoms correspond to Figure S7.

Atom	Label	q (e^-)
Cu	1	0.41780
Si	2	1.80360
N	3	-0.06370
F	4	-0.64030
F	5	-0.59730
C	6	0.06050
H	7	0.15240

Figure S8. Fragments of **SIFSIX-3-Cu** that were selected for gas phase charge fitting calculations. Label of atoms correspond to Figure §7. Atom colors: C = cyan, H = white, N = blue, F = green, Si = yellow, Cu = tan.

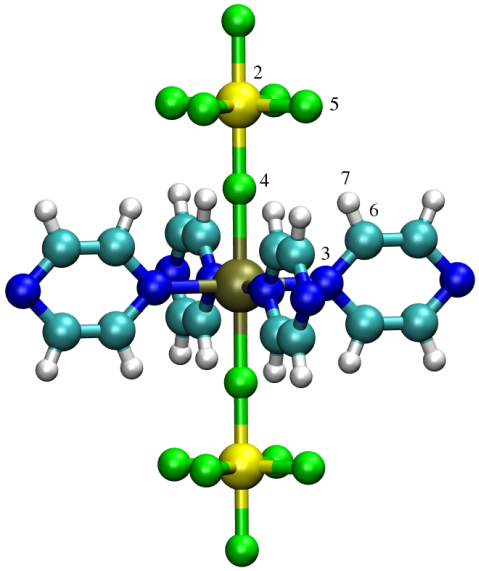

(a) Fragment 1

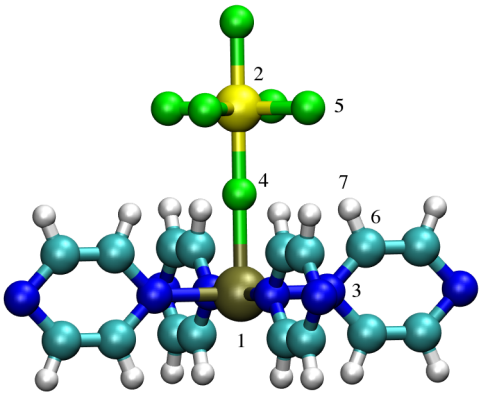

(b) Fragment 2

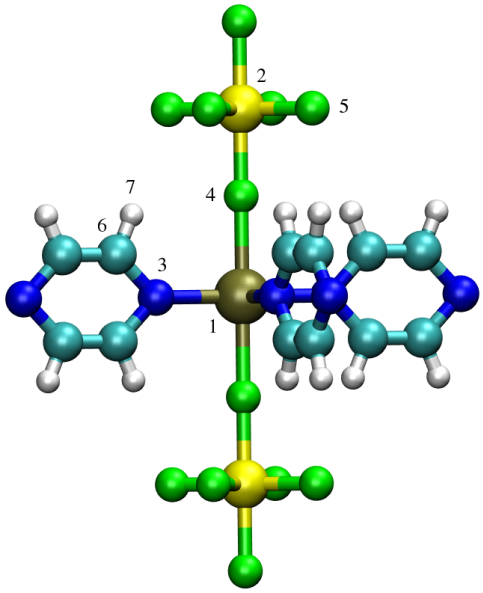

(c) Fragment 3

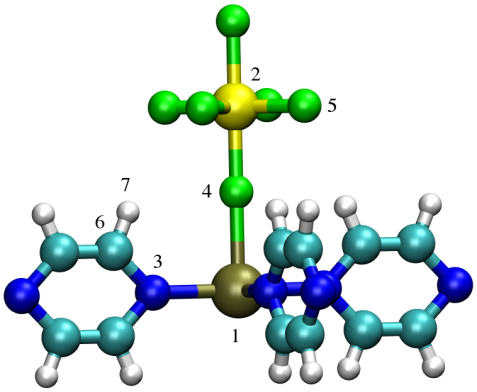

(d) Fragment 4

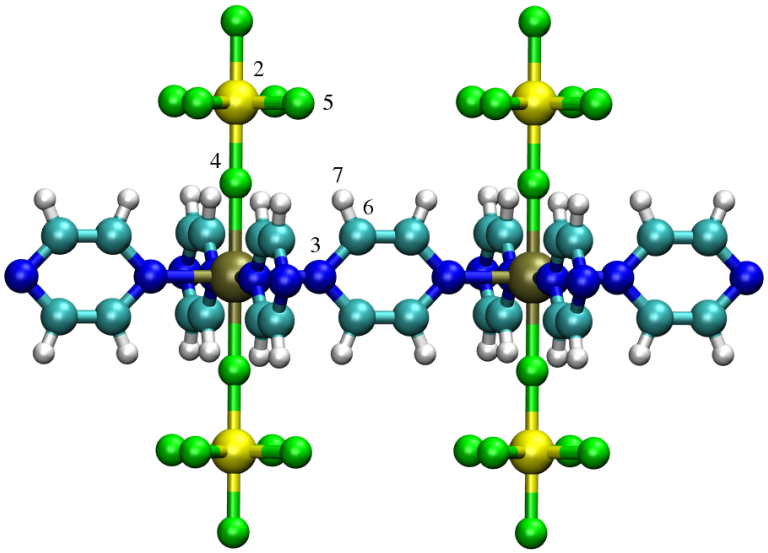

(e) Fragment 5

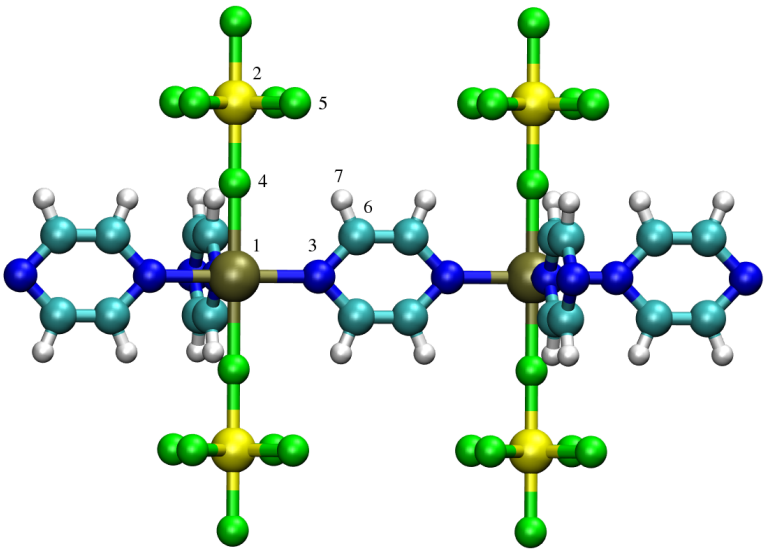

(f) Fragment 6

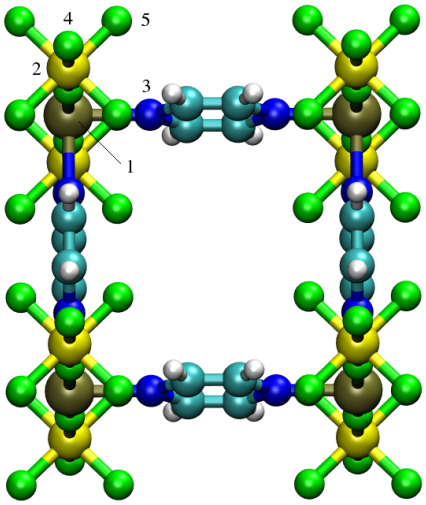

(g) Fragment 7

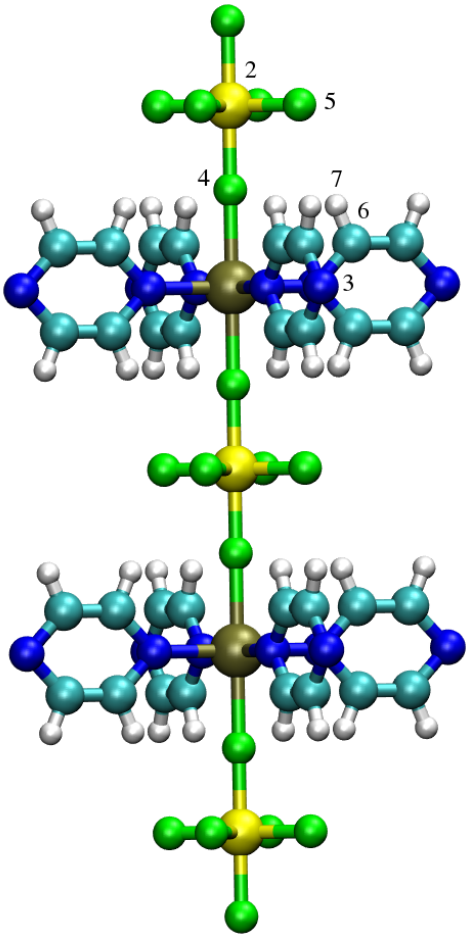

(h) Fragment 8

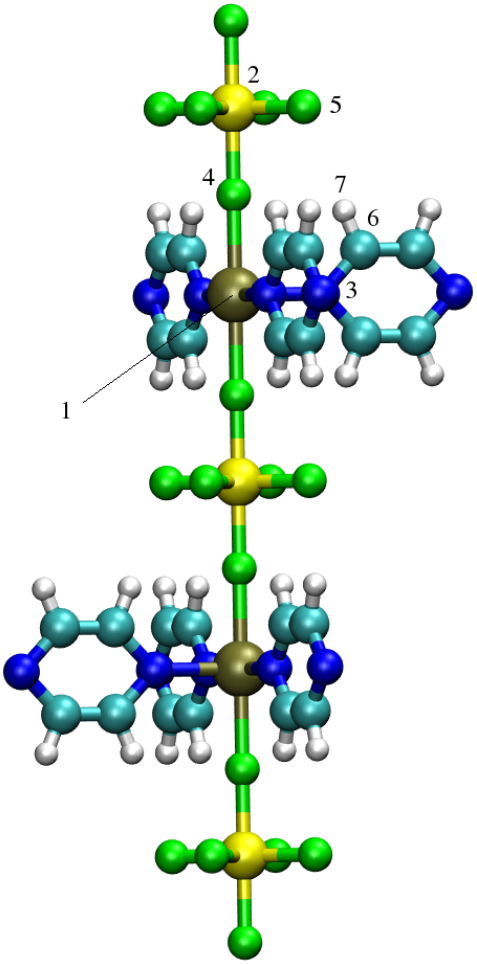

(i) Fragment 9

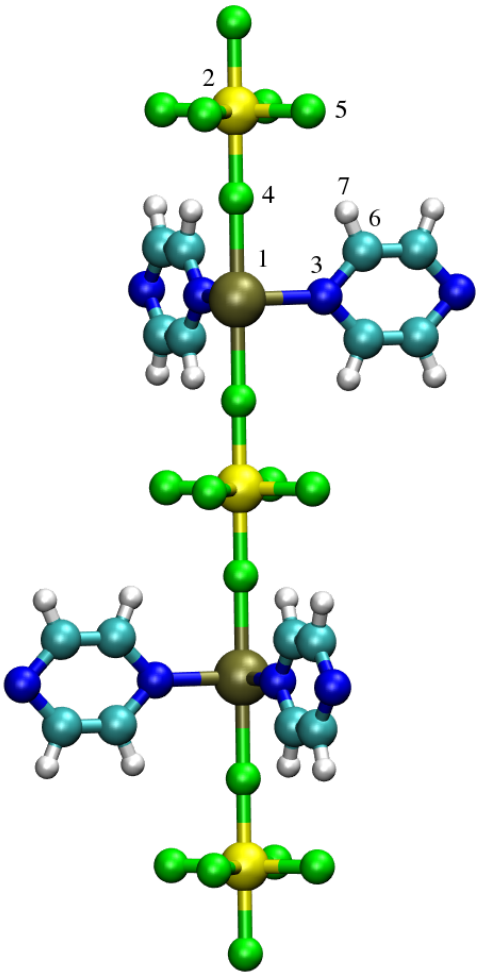

(j) Fragment 10

Theoretical Pore Volume

In addition to using the PLATON software,[38] the theoretical pore volume for all five MOMs was calculated using a previously reported simulation technique involving He.[39] The relationship between the absolute amount of sorbed molecules (N_{abs}) and the amount of sorbed molecules in excess of the number of molecules that would occupy the free pore volume at bulk gas conditions (N_{ex}) is represented by the following equation:[40]

$$N_{ex} = N_{abs} - V_p \rho_b \tag{3}$$

where V_p is the pore volume and ρ_b is the bulk phase density. For He at ambient temperatures, N_{ex} is equal to 0 because it is a non-adsorbing (or weakly adsorbing) gas. Therefore, equation 3 becomes the following:

$$V_p = \frac{N_{abs}}{\rho_b} \tag{4}$$

At low pressures, He is assumed to exhibit ideal behavior and this yields equation 4 as:

$$V_p = \frac{N_{abs} kT}{P} \tag{5}$$

where k is the Boltzmann constant, T is the temperature, and P is the pressure.
The adsorption second virial coefficient from experiment and simulation is calculated by:

$$B_{ex} = kT \lim_{P \to 0} \left(\frac{dN_{ex}}{dP} \right) \tag{6}$$

and

$$B_{abs} = kT \lim_{P \to 0} \left(\frac{dN_{abs}}{dP} \right) \tag{7}$$

Combining equations 3, 6, and 7 gives

$$B_{ex} = B_{abs} - V_p \tag{8}$$

For He, both N_{ex} and B_{ex} are equal to zero, so equation 8 becomes:

$$V_p = B_{abs} \approx kTm \tag{9}$$

where m is the slope of the essentially linear He sorption isotherm as P approaches zero.

In this work, GCMC simulations of He sorption were performed in all five SIFSIX MOMs at 298 K and pressures from 5–100 atm. The sorbate was modeled as a single–site Lennard-Jones potential that was reported previously.[41] The simulations consisted of a total of 2×10^6 Monte Carlo steps for all state points considered. The slope that was determined from the linear fitting of the resulting He sorption isotherm was used to calculate the theoretical pore volume *via* equation 9 for all five MOMs. The pore volumes that were determined through this simulation technique are compared with those calculated by PLATON for the individual SIFSIX MOMs in Table S7. It can be observed that the pore volumes that were obtained by the two methods are in very good agreement with each other for the all MOMs.

Table S7. Comparison of the theoretical pore volume (in $cm^3\ g^{-1}$) for **SIFSIX-1-Cu**, **SIFSIX-2-Cu**, **SIFSIX-2-Cu-i**, **SIFSIX-3-Zn**, and **SIFSIX-3-Cu** as determined through the PLATON software[38] and simulations of He sorption at 298 K.

	V_p ($cm^3\ g^{-1}$)	
MOM	PLATON	He Sorption
SIFSIX-1-Cu	0.683	0.682
SIFSIX-2-Cu	1.083	1.065
SIFSIX-2-Cu-i	0.263	0.259
SIFSIX-3-Zn	0.188	0.185
SIFSIX-3-Cu	0.178	0.174

Simulated CO_2 Sorption Results

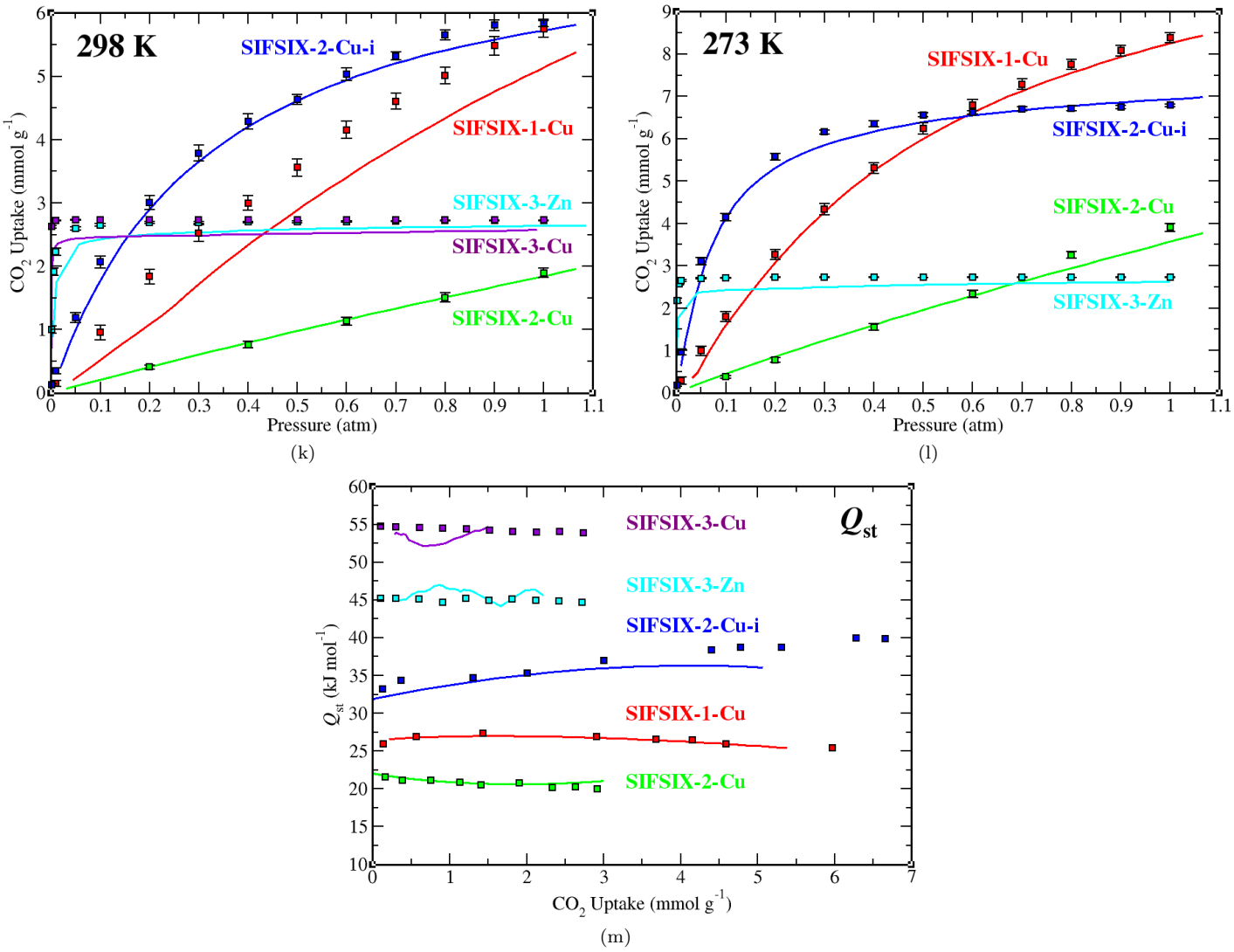

Figure S9. Low-pressure (up to 1.0 atm) CO_2 sorption isotherms at **(a)** 298 K and **(b)** 273 K and **(c)** isosteric heat of adsorption (Q_{st}) for CO_2 plotted against CO_2 uptakes for experiment (solid lines) and simulation (squares) in **SIFSIX-1-Cu** (red), **SIFSIX-2-Cu** (green), **SIFSIX-2-Cu-i** (blue), **SIFSIX-3-Zn** (cyan), and **SIFSIX-3-Cu** (violet). The experimental data for **SIFSIX-1-Cu** and **SIFSIX-3-Cu** were taken from references 2 and 5, respectively, while those for **SIFSIX-2-Cu**, **SIFSIX-2-Cu-i**, and **SIFSIX-3-Zn** were taken from reference 3. Note, experimental CO_2 sorption data for **SIFSIX-3-Cu** at 273 K is not available.

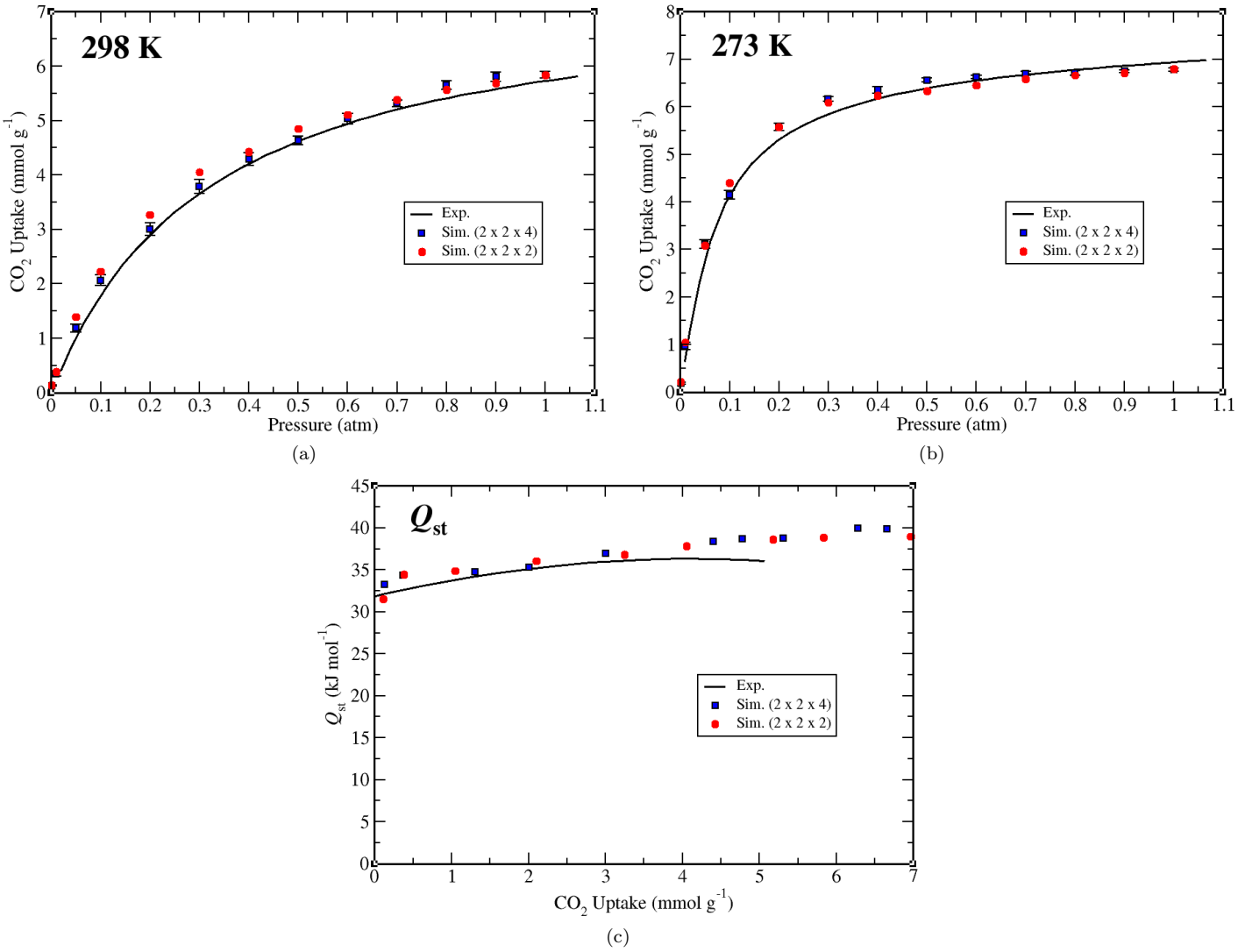

Figure S10. Low-pressure (up to 1.0 atm) CO_2 sorption isotherms at **(a)** 298 K and **(b)** 273 K and **(c)** isosteric heat of adsorption (Q_{st}) for CO_2 plotted against CO_2 uptakes in **SIFSIX-2-Cu-i** for experiment (black solid line) and simulations using a 2 × 2 × 2 (red circles) and 2 × 2 × 4 (blue squares) system cell of the MOM. The experimental data for **SIFSIX-2-Cu-i** were taken from reference 3.

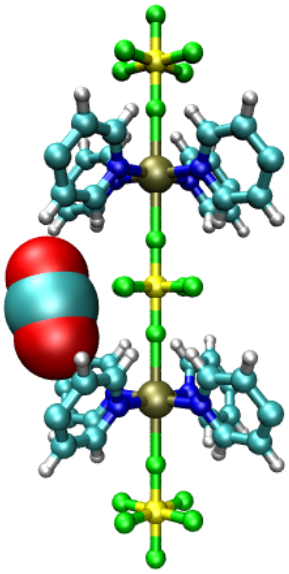

Figure S11. Molecular illustration of the CO_2 binding site about the SiF_6^{2-} pillars in **SIFSIX-1-Cu** as determined from simulation. This binding site is based on simulations in the 4,4′-bipyridine (bpy) ring configuration and equatorial fluorine atom position for the MOM as shown in Figure S2. Atom colors: C = cyan, H = white, N = blue, O = red, F = green, Si = yellow, Cu = tan.

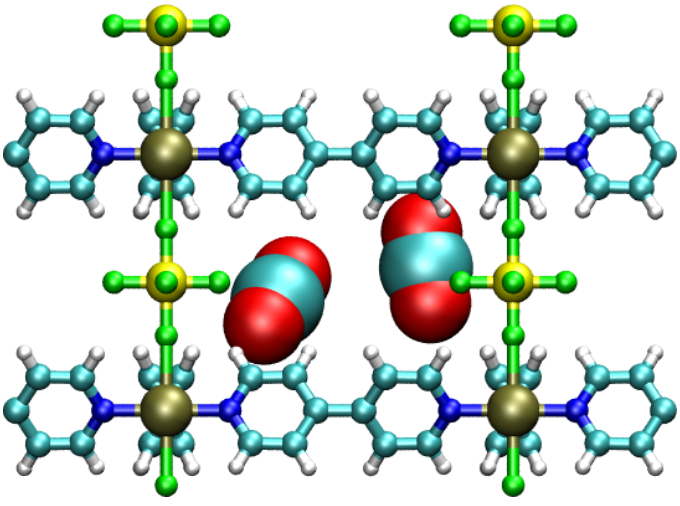

Figure S12. Molecular illustration of the roughly slipped parallel orientation of two adjacent CO_2 molecules that are sorbed onto neighboring equatorial fluorine atoms in **SIFSIX-1-Cu** as determined from simulation. Atom colors: C = cyan, H = white, N = blue, O = red, F = green, Si = yellow, Cu = tan.

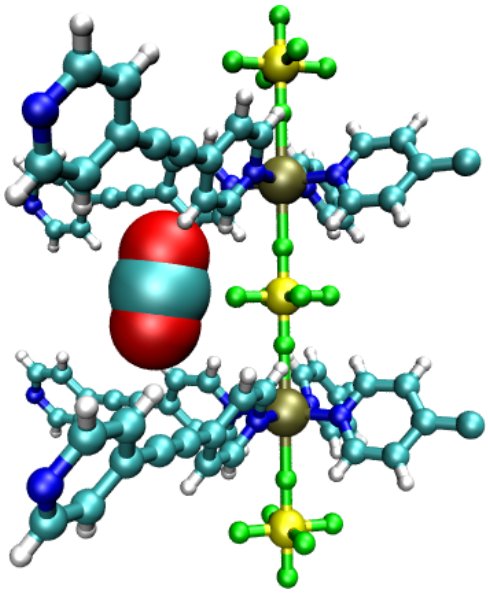

Figure S13. Molecular illustration of the CO_2 binding site about the SiF_6^{2-} pillars in **SIFSIX-2-Cu** as determined from simulation. Atom colors: C = cyan, H = white, N = blue, O = red, F = green, Si = yellow, Cu = tan.

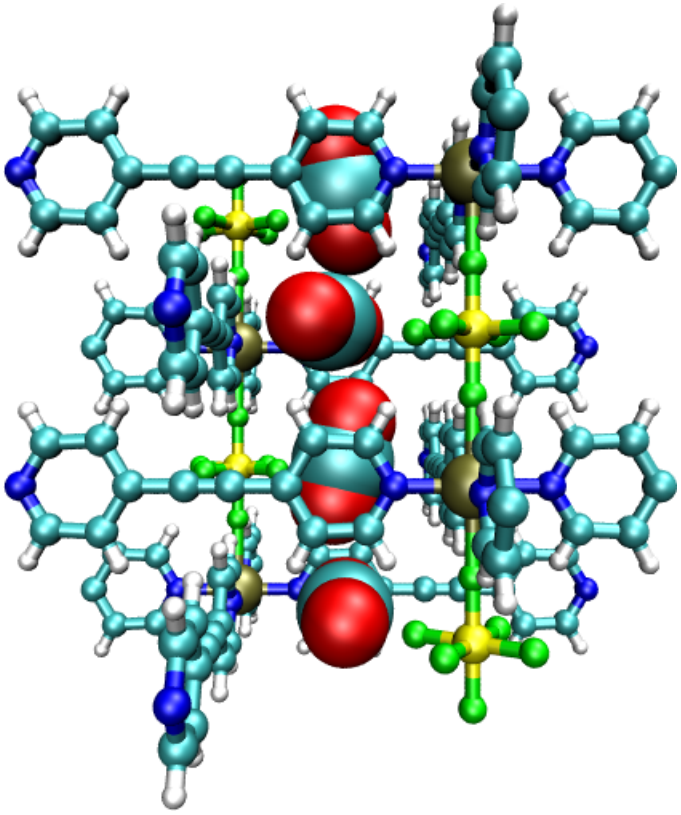

Figure S14. Molecular illustration of the alternating vertical–horizontal alignment of sorbed CO_2 molecules within a channel in **SIFSIX-2-Cu-i** as determined from simulation. Atom colors: C = cyan, H = white, N = blue, O = red, F = green, Si = yellow, Cu = tan.

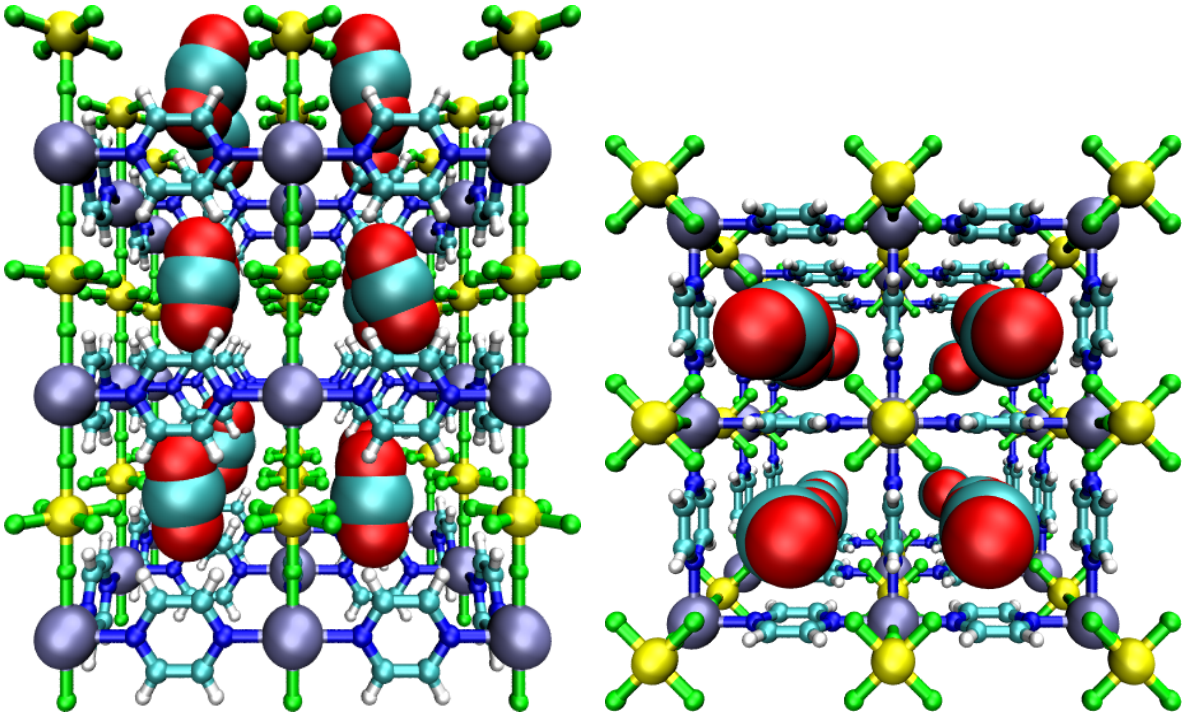

(a) (b)

Figure S15. Molecular illustration of **(a)** the a/b-axis view and **(b)** the c-axis view of the modeled $3 \times 3 \times 3$ system cell of **SIFSIX-3-Zn** at CO_2 saturation. Note, the terminal pyrazine units were removed for clarity. Atom colors: C = cyan, H = white, N = blue, O = red, F = green, Si = yellow, Zn = lavender.

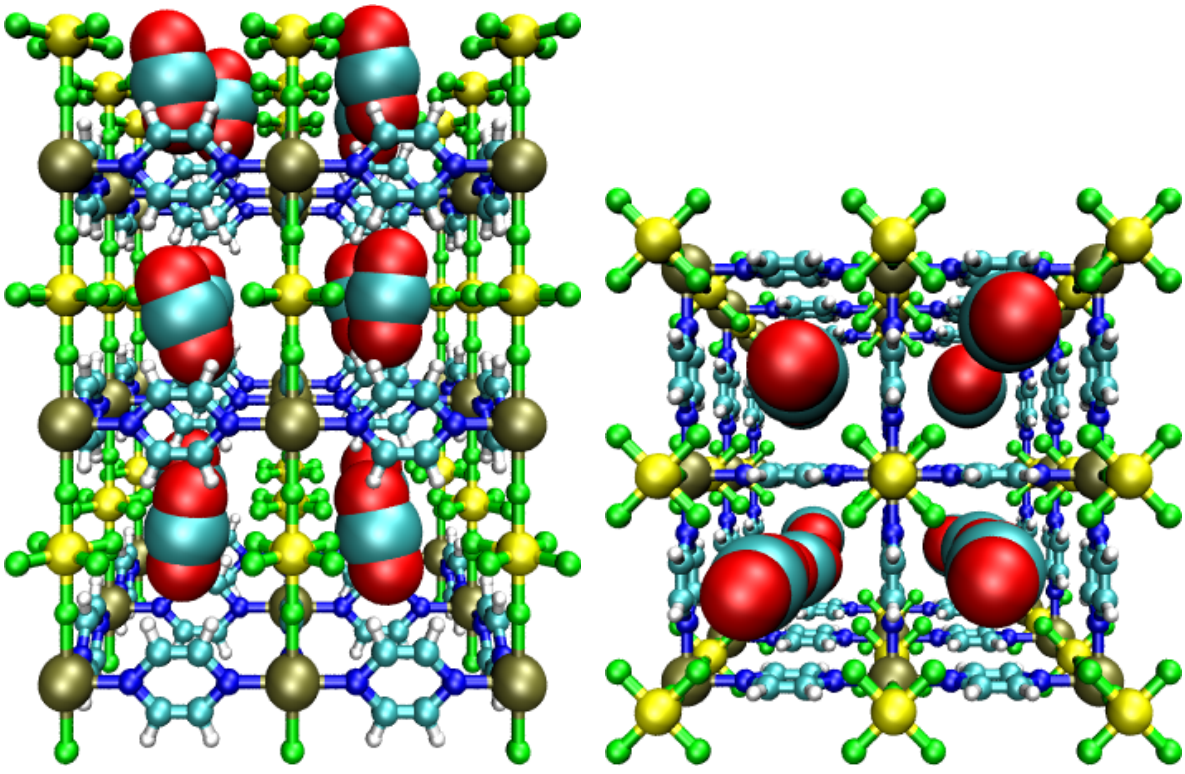

(a) (b)

Figure S16. Molecular illustration of **(a)** the a/b-axis view and **(b)** the c-axis view of the modeled $3 \times 3 \times 3$ system cell of **SIFSIX-3-Cu** at CO_2 saturation. Note, the terminal pyrazine units were removed for clarity. Atom colors: C = cyan, H = white, N = blue, O = red, F = green, Si = yellow, Cu = tan.

[1] N. Metropolis, A. W. Rosenbluth, M. N. Rosenbluth, A. H. Teller and E. Teller, *J. Chem. Phys.*, 1953, **21**, 1087–1092.
[2] S. D. Burd, S. Ma, J. A. Perman, B. J. Sikora, R. Q. Snurr, P. K. Thallapally, J. Tian, L. Wojtas and M. J. Zaworotko, *J. Am. Chem. Soc.*, 2012, **134**, 3663–3666.
[3] P. Nugent, Y. Belmabkhout, S. D. Burd, A. J. Cairns, R. Luebke, K. Forrest, T. Pham, S. Ma, B. Space, L. Wojtas, M. Eddaoudi and M. J. Zaworotko, *Nature*, 2013, **495**, 80–84.
[4] K. Uemura, A. Maeda, T. K. Maji, P. Kanoo and H. Kita, *Eur. J. Inorg. Chem.*, 2009, **2009**, 2329–2337.
[5] O. Shekhah, Y. Belmabkhout, Z. Chen, V. Guillerm, A. Cairns, K. Adil and M. Eddaoudi, *Nature Commun.*, 2014, **5**, 4228.
[6] D. A. McQuarrie, *Statistical Mechanics*, University Science Books, Sausalito, CA, 2000.
[7] D. Frenkel and B. Smit, *Understanding Molecular Simulation: From Algorithms to Applications*, Academic Press, New York, 2002.
[8] D.-Y. Peng and D. B. Robinson, *Ind. Eng. Chem. Fundam.*, 1976, **15**, 59–64.
[9] J. Jones, *Proc. R. Soc. A*, 1924, **106**, 463–477.
[10] P. P. Ewald, *Ann. Phys.*, 1921, **369**, 253–287.
[11] B. A. Wells and A. L. Chaffee, *J. Chem. Theory Comput.*, 2015, **11**, 3684–3695.
[12] J. Applequist, J. R. Carl and K.-K. Fung, *J. Am. Chem. Soc.*, 1972, **94**, 2952–2960.
[13] B. Thole, *Chem. Phys.*, 1981, **59**, 341–350.
[14] K. A. Bode and J. Applequist, *J. Phys. Chem.*, 1996, **100**, 17820–17824.
[15] K. McLaughlin, C. R. Cioce, T. Pham, J. L. Belof and B. Space, *J. Chem. Phys.*, 2013, **139**, 184112.
[16] M. P. Allen and D. J. Tildesley, *Computer Simulation of Liquids*, Oxford University Press, Oxford, United Kingdom, 1989.
[17] A. L. Mullen, T. Pham, K. A. Forrest, C. R. Cioce, K. McLaughlin and B. Space, *J. Chem. Theory Comput.*, 2013, **9**, 5421–5429.
[18] F. Siperstein, A. Myers and O. Talu, *Mol. Phys.*, 2002, **100**, 2025–2030.
[19] D. Wolf, P. Keblinski, S. R. Phillpot and J. Eggebrecht, *J. Chem. Phys.*, 1999, **110**, 8254–8282.
[20] D. Nicholson and N. G. Parsonage, *Computer Simulation and the Statistical Mechanics of Adsorption*, Academic Press, London, 1982.
[21] J. L. Belof and B. Space, *Massively Parallel Monte Carlo (MPMC)*, Available on GitHub, 2012, `https://github.com/mpmccode/mpmc`.
[22] W. L. Jorgensen, D. S. Maxwell and J. Tirado-Rives, *J. Am. Chem. Soc.*, 1996, **118**, 11225–11236.
[23] P. T. van Duijnen and M. Swart, *J. Phys. Chem. A*, 1998, **102**, 2399–2407.
[24] P. Nugent, V. Rhodus, T. Pham, B. Tudor, K. Forrest, L. Wojtas, B. Space and M. Zaworotko, *Chem. Commun.*, 2013, **49**, 1606–1608.
[25] T. Pham, K. A. Forrest, K. McLaughlin, B. Tudor, P. Nugent, A. Hogan, A. Mullen, C. R. Cioce, M. J. Zaworotko and B. Space, *J. Phys. Chem. C*, 2013, **117**, 9970–9982.
[26] K. A. Forrest, T. Pham, A. Hogan, K. McLaughlin, B. Tudor, P. Nugent, S. D. Burd, A. Mullen, C. R. Cioce, L. Wojtas, M. J. Zaworotko and B. Space, *J. Phys. Chem. C*, 2013, **117**, 17687–17698.
[27] K. A. Forrest, T. Pham, P. Nugent, S. D. Burd, A. Mullen, L. Wojtas, M. J. Zaworotko and B. Space, *Cryst. Growth. Des.*, 2013, **13**, 4542–4548.
[28] K. A. Forrest, T. Pham, K. McLaughlin, J. L. Belof, A. C. Stern, M. J. Zaworotko and B. Space, *J. Phys. Chem. C*, 2012, **116**, 15538–15549.
[29] M. Valiev, E. Bylaska, N. Govind, K. Kowalski, T. Straatsma, H. V. Dam, D. Wang, J. Nieplocha, E. Apra, T. Windus and W. de Jong, *Comput. Phys. Commun.*, 2010, **181**, 1477–1489.
[30] W. D. Cornell, P. Cieplak, C. I. Bayly, I. R. Gould, K. M. Merz, D. M. Ferguson, D. C. Spellmeyer, T. Fox, J. W. Caldwell and P. A. Kollman, *J. Am. Chem. Soc.*, 1995, **117**, 5179–5197.
[31] W. J. Stevens, H. Basch and M. Krauss, *J. Chem. Phys.*, 1984, **81**, 6026–6033.
[32] P. J. Hay and W. R. Wadt, *J. Chem. Phys.*, 1985, **82**, 270–283.
[33] L. A. LaJohn, P. A. Christiansen, R. B. Ross, T. Atashroo and W. C. Ermler, *J. Chem. Phys.*, 1987, **87**, 2812–2824.
[34] L. E. Chirlian and M. M. Francl, *J. Comput. Chem.*, 1987, **8**, 894–905.
[35] C. M. Breneman and K. B. Wiberg, *J. Comput. Chem.*, 1990, **11**, 361–373.
[36] D.-L. Chen, A. C. Stern, B. Space and J. K. Johnson, *J. Phys. Chem. A*, 2010, **114**, 10225–10233.
[37] A. C. Stern, *Ph.D. thesis*, University of South Florida, 2010.
[38] A. L. Spek, *Acta Cryst.*, 2009, **D65**, 148–155.
[39] O. Talu and A. L. Myers, *AIChE J.*, 2001, **47**, 1160–1168.
[40] A. L. Myers and P. A. Monson, *Langmuir*, 2002, **18**, 10261–10273.
[41] G. Garberoglio, A. I. Skoulidas and J. K. Johnson, *J. Phys. Chem. B*, 2005, **109**, 13094–13103.